ROBUST BEAMFORMER WEIGHT DESIGN FOR BROADBAND MATCHED-FIELD PROCESSSING

Kerem Harmanci and Jeffrey L. Krolik

Department of Electrical and Computer Engineering
Duke University, Durham, NC, 27708, USA
jk@ee.duke.edu

ABSTRACT

Matched-field beamforming has been proposed for localizing wideband acoustic sources in uncertain underwater channels. While adaptive matched-field beamforming provides adequate sidelobe suppression for stronger sources, at low signal-to-noise ratios it converges to its quiescent response, in this case the Bartlett beamformer, which has unacceptably high sidelobe levels. In this paper, a design method is presented for reducing non-adaptive matched-field beamformer sidelobe levels given a sufficiently large observation-time-bandwidth product. The proposed α-beamformer incoherently averages narrowband matched-field beamformer output power over the signal band after a trade-off has been performed at each frequency to achieve better sidelobe suppression at the expense of some reduction in gain against diffuse noise. Simulations and results with Mediterranean vertical array data indicate that the wideband α-beamformer can provide improved sidelobe suppression versus conventional techniques.

1. INTRODUCTION

Matched-field beamforming exploits full-field models of complex multipath propagation to perform acoustic source localization in range and depth. A major difficulty facing conventional (a.k.a. Bartlett) matched-field beamformers are their high sidelobe levels. Minimum variance (MV) adaptive beamforming has been proposed to suppress sidelobes in high signal-to-noise ratio (SNR) scenarios [1]. At low SNR's, however, the MV adaptive beamformer converges to the quiescent Bartlett weight vector, whose sidelobe levels are often less than 1 dB down.

For wideband signals, incoherent averaging of narrowband ambiguity surfaces provides some reduction in sidelobe levels but requires at least one or two octaves of bandwidth in order for ambiguity function sidelobes to decorrelate over frequency. To achieve improved sidelobe suppression with less bandwidth, the approach taken in this paper is to design non-adaptive beamformer weights which trade narrowband signal-to-diffuse-noise gain for lower average sidelobe behavior at each frequency. Since the diffuse noise component of the ambiguity surface is uncorrelated even for small frequency separations, the loss in diffuse noise gain can be overcome by incoherent averaging over frequency using even moderate signal bandwidths.

2. ACOUSTIC PROPAGATION MODEL

Consider an acoustic source in a shallow-water ocean channel. A T_s second "snapshot" of the acoustic field may be represented by its Fourier series coefficients at frequencies, $\omega_i = \frac{2\pi i}{T_s}$, across the signal band. Using the adiabatic normal mode solution to the wave equation, the complex Fourier series coefficient at frequency ω_i of the field measured at depth z from a distant source at range r_s and depth z_s can be expressed as:

$$p(z; r_s, z_s, \omega_i) = a(\omega_i)\sqrt{2\pi}\sum_{n=1}^{N}\frac{\phi_n^{(0)}(z)\phi_n(z_s)}{\sqrt{k_n r_s}}e^{-jk_n r_s} \quad (1)$$

where, $\phi_n(z_s)$ and $\phi_n^{(0)}(z)$ are the modal depth eigenfunctions at the source and receiver, respectively, and the $k_n = \frac{1}{r_s}\int_0^{r_s} k_n(r)dr$, are range-averaged complex modal horizontal wavenumbers and $a(\omega_i)$ is the source amplitude.

For a vertical array of M sensors, a $M \times 1$ frequency-domain vector of sensor outputs for the k^{th} snapshot at frequency ω_i, denoted $\mathbf{x}_k$, can be expressed by evaluating Eq.1 at the sensor depths, z_1, ..., z_M. Writing the result in matrix notation gives:

$$\mathbf{x}_k(\omega_i) = a_k(\omega_i)\mathbf{U}\mathbf{s}(r_s, z_s) + \eta_k \quad (2)$$

where the $(m,n)^{th}$ element of the $M \times N$ matrix $\mathbf{U}$ is $\phi_n^{(0)}(z_m)$ and the n^{th} element of the modal amplitude vector $\mathbf{s}(r_s, z_s)$ is $\sqrt{2\pi}\frac{\phi_n^{(0)}(z_s)e^{-jk_n r_s}}{\sqrt{k_n r_s}}$, η_k is diffuse additive background noise. For passive sonar applications, both the a_k and the elements of η_k can be modeled as complex zero-mean Gaussian random variables. A complete observation of the wideband data consists of a set of uncorrelated snapshots, $\mathbf{x}_k(\omega_i)$, for $i = 1, ..., N_f$ and $k = 1, ..., N_s$. Note that snapshots are uncorrelated both over k and i.

A shallow-water Mediterranean region is the model of interest [1]. The nominal baseline environmental parameter values are taken from [2]. However, the actual values of the geoacoustic parameters are uncertain. As in [2], the parameter values are assumed to lie within the following ranges: bathymetry(125-130 m.); upper sediment sound speed (1450-1550 m/s), lower sediment sound speed (1500-1600 m/s); sediment density (1.2-2.2 g/cm^3); sediment attenuation (0.0-0.4 dB/λ); sediment thickness (0.0 - 6.0 m); sub-bottom sound-speed (1550-1650 m/s); sub-bottom density(1.2-2.2 g/cm^3); sub-bottom attenuation (0.0-0.4 db/λ).

3. DESIGN TRADE-OFFS

Matched-field processing consists of beamforming using the signal wavefront model described by Eq. 2. The narrowband ambiguity surface is the beamformer output power plotted as a function of hypothesized $\theta = [r_s, z_s]$. For wideband source signals, incoherent averaging of narrowband ambiguity surfaces across frequency can reduce the level of ambiguous sidelobes but the improvement is limited by the constituent narrowband beamformer sidelobe responses as well as their sensitivity to environmental mismatch. In this paper, narrowband beamformer weights are designed to achieve lower sidelobe levels by trading signal-to-noise ratio gain against uncorrelated noise (G_{SNR}) defined by:

$$G_{SNR} = \frac{\mathbf{w}^\dagger \mathbf{R}_L \mathbf{w}}{\mathbf{w}^\dagger \mathbf{w}} \tag{3}$$

versus average output signal-to-interference ratio (SIR_o)

$$SIR_o = \frac{\mathbf{w}^\dagger \mathbf{R}_L \mathbf{w}}{\mathbf{w}^\dagger \mathbf{R}_{SL} \mathbf{w}}. \tag{4}$$

where $R_L = E[\mathbf{d}(\theta_L)\mathbf{d}(\theta_L)^\dagger]$ is the correlation matrix of wavefronts $\mathbf{d}(\theta) = \mathbf{U}\mathbf{s}(\theta)$ received from the hypothesized location θ_L averaged over the uncertain environmental parameters. The matrix $\mathbf{R}_{SL} = E_\theta[E[\mathbf{d}(\theta)\mathbf{d}(\theta)^\dagger]]$ is the correlation matrix of wavefronts in the sidelobe region Θ_{SL} where the outer expectation is taken over θ uniformly distributed over Θ_{SL}. In the case of plane-wave beamformers, this trade-off is performed by well-known designs which increase mainlobe width (which decreases G_{SNR}) to achieve lower sidelobe levels (which increases SIR_o).

The effect of this trade-off on performance in finite observation-time-signal-bandwidth product (TBP) scenarios can be illustrated by formulating the localization problem as a binary detection problem. For analytical tractability, the wideband analysis performed here assumes the effect of $N_f > 1$ is simply to increase the effective number of uncorrelated snapshots available for incoherent averaging. Thus define,

$$H_0: \quad \mathbf{x}_k = \mathbf{d}(\theta) + \eta_k \qquad \theta \in \Theta_{SL} \tag{5}$$

$$H_1: \quad \mathbf{x}_k = \mathbf{d}(\theta_L) + \eta_k \tag{6}$$

for $k = 1, ..., N_s N_f$ where TBP $= N_s N_f$ and model $\mathbf{d}$ as a zero-mean complex Gaussian random vector with covariance matrix $\mathbf{R}_{SL}$ and $\mathbf{R}_L$ under H_0 and H_1, respectively. The test statistic used to decide H_0 versus H_1 is the incoherently averaged beamformer output power which can be expressed as:

$$Z = \frac{1}{\text{TBP}} \sum_{k=1}^{\text{TBP}} \left|\mathbf{w}^\dagger \mathbf{x}_k\right|^2. \tag{7}$$

A useful performance measure for this hypothesis testing problem is the Deflection Index, DI defined as ,

$$DI = \frac{E[Z|H_1] - E[Z|H_0]}{\sqrt{\text{Var}[Z|H_0]}}. \tag{8}$$

Given the above definitions, an expression for the Deflection Index can be derived in terms of the input SNR $\rho_i = \frac{\sigma_s^2}{\sigma_n^2}$, G_{SNR}, and $Y = \frac{1}{SIR_o}$. The resulting formula is,

$$DI = \frac{\sqrt{N_s N_f}\,\rho_i G_{SNR}(1-Y)}{\sqrt{(N_s N_f + 2)(\rho_i G_{SNR} Y)^2 + 2(\rho_i G_{SNR} Y) + 1}}. \tag{9}$$

A good design can be obtained by using choosing the pair (G_{SNR}, SIR_o) that maximizes DI out of those pairs achievable by the environment and design method at hand. Typically, at low SNR and large TBP, DI is increased by reducing G_{SNR} to increase SIR_o. For example, in the limit as TBP $\to \infty$, $DI = \frac{1-Y}{Y}$, independent of G_{SNR}.

4. THE α-BEAMFORMER

In this section, a beamformer design method is presented which achieves the best average SIR_o for a specified gain against diffuse noise. Since the signal wavefront is assumed random, this is achieved by minimizing $\mathbf{w}^\dagger \mathbf{R}_{SL} \mathbf{w}$ subject to the quadratic constraint of fixed $\mathbf{w}^\dagger \mathbf{R}_L \mathbf{w}$. In order to ensure that the response of the beamformer to uncorrelated noise is flat as a function of hypothesized source location, an additional equality constraint is required to ensure $\mathbf{w}^\dagger \mathbf{w}$ is constant. Thus at each frequency, ω_i, and hypothesized source location, θ_L, the algorithm solves for the beamformer weight vector $\mathbf{w}$ which satisfies:

$$\min_{\mathbf{w}} \mathbf{w}^\dagger \mathbf{R}_{SL} \mathbf{w} \tag{10}$$

subject to

$$\mathbf{w}^\dagger \mathbf{R}_L \mathbf{w} = \alpha \tag{11}$$

$$\mathbf{w}^\dagger \mathbf{w} = 1. \tag{12}$$

where $\alpha = G_{SNR}$. Note that unlike traditional Chebyshev designs, the α-beamformer minimizes the average rather than the maximum sidelobe level. The minimax criterion was not employed since in typical matched-field processing scenarios, the maximum sidelobe is nearly a grating-lobe of the beamformer and trying to suppress it exclusively results in a huge sacrifice in gain against diffuse noise.

An interesting feature of this optimization is the incorporation of two quadratic constraints. Solution of this problem was performed by sequential quadratic programming (SQP) [3], using an initial guess chosen to be the unit norm beamformer that maximizes G_{SNR}, i.e. the dominant eigenvector of $\mathbf{R}_L$. However, this choice does not always satisfy both quadratic constraints so in the implementation, the first constraint is given by the inequality ($\mathbf{w}^\dagger \mathbf{R}_L \mathbf{w} \geq \alpha$). The final solution is generally at the edge of the region defined by the inequality constraint. Hence the final solution does satisfy the equality constraints. In some cases, the final solution does not appear at the expected edge, so the constraint $\mathbf{w}^\dagger \mathbf{w} \leq 1$ is altered to an equality constraint, but convergence to the solution is slower.

The α-Beamformer $\mathbf{w}_\alpha$ can also be used as the quiescent response of an adaptive minimum variance (MV) matched-field beamformer such as the MV-EPC method described in [1]. Incorporating the quiescent weights, $\mathbf{w}_\alpha$, into the

MV-EPC design is achieved using the method of Tseng and Griffiths [4]. The approach consists of using linear constraints for the MV beamformer given by $\mathbf{H}_\alpha^\dagger \mathbf{w} = \mathbf{e}_1$ where $\mathbf{H}_\alpha = [\mathbf{w}_\alpha, \bar{\mathbf{H}}]$, and $\bar{\mathbf{H}}$ are the dominant eigenvectors of $\bar{\mathbf{R}}_d$. The matrix $\bar{\mathbf{R}}_d$ is formed by taking $\bar{\mathbf{R}}_d = (\mathbf{I} - \mathbf{P}_{\mathbf{w}_\alpha})^\dagger \mathbf{R}_d (\mathbf{I} - \mathbf{P}_{\mathbf{w}_\alpha})$ where $P_{w_\alpha} = \mathbf{w}_\alpha (\mathbf{w}_\alpha{}^\dagger \mathbf{w}_\alpha)^{-1} \mathbf{w}_\alpha{}^\dagger$ The resulting narrowband α-MV-EPC beamformer output power is given by

$$Z_{\alpha\text{-MV-EPC}}(r,z) = \mathbf{e}_1^\dagger (\bar{\mathbf{H}}_\alpha^\dagger \mathbf{R}_{\mathbf{xx}} \bar{\mathbf{H}}_\alpha)^{-1} \mathbf{e}_1. \qquad (13)$$

and the wideband α-MV-EPC ambiguity surface is obtained by incoherently averaging Eq. 13 over frequency.

5. RESULTS

In this section, the proposed algorithms are compared with conventional methods using simulated and experimental data from the Mediterranean Sea. In order to minimize computational requirements, Monte Carlo simulations were carried out for range estimation only, assuming source depth was known. An uncertain environment with parameters uniformly distributed in the intervals indicated in Section 2 was assumed. Note that the maximum eigenvalue of $\mathbf{R}(\theta_L)$ is a varying function of θ_L. Hence the largest possible α that can be chosen for a uniform G_{SNR} design is the minimum over θ_L of maximum eigenvalues.

As a measure of the severity of the sidelobes for a particular ambiguity surface, a performance metric based on the deflection index is used. The "detectability", D_y, is defined here by:

$$D_y = \frac{Z_L - \overline{Z}_{SL}}{\sqrt{(\overline{Z}_{SL} - Z_{SL})^2}} \qquad (14)$$

where L denotes the ambiguity surface peak in the neighborhood of the true source location and SL denotes the sidelobe region. In Eq. 14 the overbar signifies an arithmetical average over Θ_{SL} for a particular ambiguity function estimate. Note that D_y quantifies the distance between the ambiguity surface peak and the average sidelobe level normalized by the variability in the sidelobe region. The other performance measure considered here is probability of correct localization which is determined by the proportion of estimates which fall within $\pm$ 300 m. in range from the true source position.

The performance of the α-beamformer is compared with the conventional Bartlett method in Table 1. The results indicate that the α-beamformer consistently outperforms Bartlett in terms of detectability and probability of correct localization for both TBP = 1000 as well as infinite TBP. The detectability improvement was as much as 6 dB.

The detectability performance of the Bartlett, the α-beamformer, the conventional MV-EPC, and α-MV-EPC are plotted as a function of SNR_i in Figure 1. Observe that the α-beamformer outperforms the Bartlett significantly in detectability. This is an expected result since Bartlett beamformer maximizes look location SNR gain and ignores sidelobe behavior, while the α trades SNR gain to achieve better sidelobe suppression. Note that at low SNR, the adaptive and non-adaptive beamformers have similar performance. The improved performance of the α-MV-EPC at low SNR is due to its superior quiescent response. At input SNR's greater than -20 dB the adaptive beamformers perform better than their quiescent weights because at these SNR's they can effectively estimate and suppress signals in the sidelobe region.

The results of matched-field processing with Mediterranean vertical array data [2] provided by the NATO SACLANT Center are shown in Figure 2. An acoustic source radiating pseudo-random noise over the band from 160 to 180 Hz. was received at a vertical array of 48 sensors which spans the 127 m. deep ocean channel. Ambiguity functions were computed for ranges from 1000 m. to 8000 m. with a 50 m. sampling interval and at depths from 2 m to 127 m with 1.3 m sampling interval. A total of 25 time snapshots and 21 frequencies giving a TBP = 525 were used to produce each ambiguity surface. The true source location was at a range 6600 m. and depth 68m., respectively. Figure 2 illustrates typical ambiguity surfaces obtained using the original MV-EPC beamformer (a) and the α-MV-EPC Beamformer (b) with $\alpha = \min_{\theta_L} \lambda_{max}$. Note that the sidelobe levels are lower for α-MV-EPC, particularly at lower ranges where the uncertainty in the channel causes less deleterious wavefront perturbations. The detectability, D_y, for these surfaces is 12.08 dB for the MV-EPC versus 15.33 dB for the α-MV-EPC. In terms of source localization, the MV-EPC estimate was 6300 m and 63 m while the α-MV-EPC estimate was 6150 m and 60 m. Note that both methods produced similarly biased source location estimates, the cause of which is discussed in [1].

6. CONCLUSION

A non-adaptive robust beamformer design technique, the α-Beamformer, has been presented which permits trade-offs between SNR gain against diffuse noise versus sidelobe suppression. Analyses with simulated and real data indicate that given sufficient observation-time-bandwidth product, exploiting this trade-off can improve source detectability and probability of correct localization.

This work was supported by NraD/ONR under contract number N66001-95-C-6032. The authors would like to thank Dr. D. Gingras of NRaD for providing the NATO SACLANT data.

REFERENCES

[1] J. L. Krolik, "The performance of matched-field beamformers with mediterranean vertical array data," *IEEE Trans.on Signal Processing*, vol. 44, pp. 2605–2611, October 1996.

[2] P. Gingras, D. F.; Gerstoft, "Inversion for geometric and geoacoustic parameters in shallow water: Experimental results," *J. Acoust. Soc. Am.*, vol. 97, pp. 3589–3598, June 1995.

[3] P. E. Gill, W. Murray, and M. H. Wright, *Practical Optimization*. London: Academic Press, 1981.

[4] C.-Y. Tseng and L. J. Griffiths, "A unified approach to the design of linear constraints in minimum variance adaptive beamformers," *Ieee Trans on Antennas Propagat.*, vol. 40, pp. 1533–1542, December 1992.

	Bartlett		α-Beamformer	
SNR_i [dB]	P_{CL}	$E[D_y]$	P_{CL}	$E[D_y]$
0	0.69	1.10	0.76	3.96
-5	0.69	1.10	0.75	3.96
-10	0.69	1.10	0.75	3.94
-15	0.70	1.09	0.75	3.85
-20	0.68	1.02	0.74	3.20
-25	0.46	0.74	0.52	1.70
-30	0.19	0.33	0.15	0.53
-35	0.15	0.06	0.11	0.18
-40	0.11	0.04	0.10	0.07
∞ snapshots	0.70	1.10	0.76	3.99

Table 1. Performance Comparison of non-adaptive algorithms in terms of P_{CL} and $E[D_y]$ with a Monte-Carlo simulation for SACLANT environment with 500 realizations and TBP = 1000 for each measurement. $\alpha = \min_{\theta_L} \lambda_{max}$.

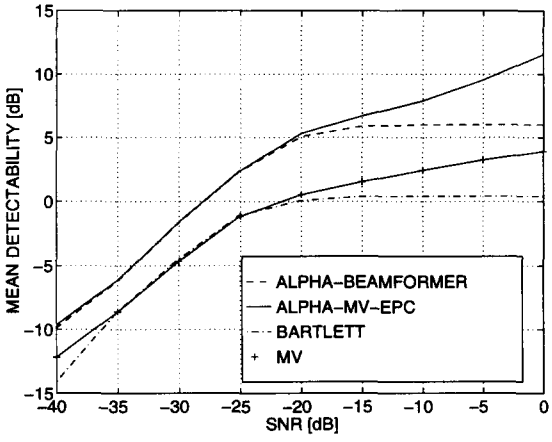

Figure 1. Performance comparison of MV-beamformers and their quiescents as a function of SNR_i for UE with finite TBP (1000 snapshots, single frequency) in terms of Detectability. Here, $\alpha = \min_{\theta_L} \lambda_{max}$, 500 realizations of the environment were taken.

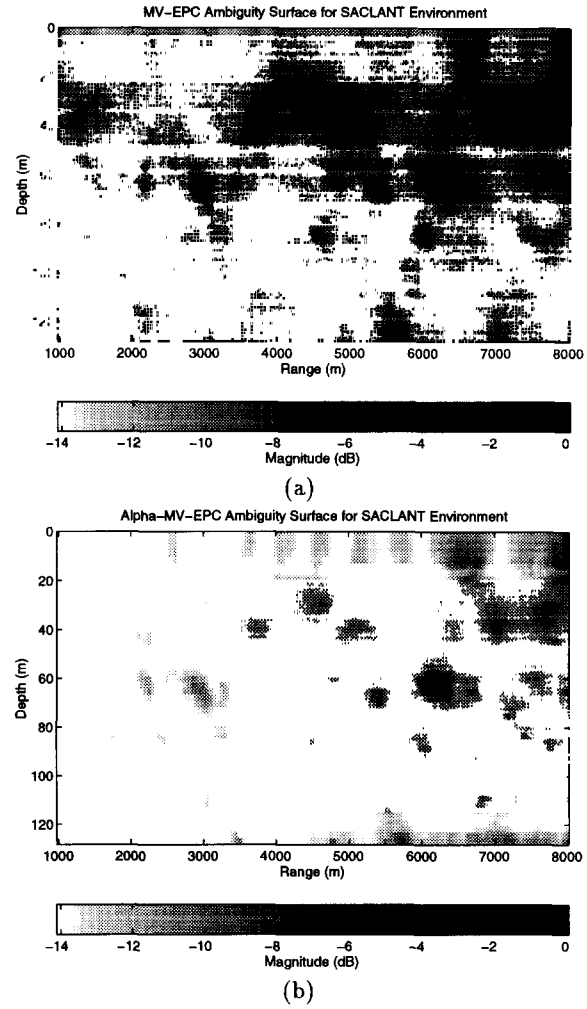

Figure 2. Ambiguity surfaces on Experimental SACLANT Data. 25 Snapshots used for data matrix. Data was processed for 21 frequencies between 160 and 180 Hz. For beamformer design, α was chosen as $\min_{\theta_L} \lambda_{max}$ The graphs correspond to the methods: (a) MV-EPC, (b) MV-EPC with α-BEAMFORMER quiescent response.